APSB
2022

ORIGINAL ARTICLE

Nuclear TIGAR mediates an epigenetic and metabolic autoregulatory loop *via* NRF2 in cancer therapeutic resistance

Hong Wang[a], Qianqian Wang[a], Guodi Cai[a], Zhijian Duan[b],
Zoann Nugent[c], Jie Huang[d],[*], Jianwei Zheng[a],
Alexander D. Borowsky[e], Jian Jian Li[f], Peiqing Liu[a,g],
Hsing-Jien Kung[b,h], Leigh Murphy[c], Hong-Wu Chen[b,h],[*],
Junjian Wang[a,g],[*]

[a]*School of Pharmaceutical Sciences, Sun Yat-sen University, Guangzhou 510006, China*
[b]*Department of Biochemistry and Molecular Medicine, University of California, Davis, Sacramento, CA 95817, USA*
[c]*Research Institute in Oncology and Hematology, University of Manitoba and CancerCare Manitoba, Winnipeg R3E 0V9, Canada*
[d]*Guangdong Lung Cancer Institute, Guangdong Provincial Key Laboratory of Translational Medicine in Lung Cancer, Guangdong Provincial People's Hospital and Guangdong Academy of Medical Sciences, Guangzhou 510080, China*
[e]*Department of Pathology and Laboratory Medicine, University of California, Davis, Sacramento, CA 95817, USA*
[f]*Department of Radiation Oncology, University of California, Davis, Sacramento, CA 95817, USA*
[g]*National-Local Joint Engineering Laboratory of Druggability and New Drugs Evaluation, Guangdong Provincial Key Laboratory of New Drug Design and Evaluation, Sun Yat-sen University, Guangzhou 510006, China*
[h]*UC Davis Comprehensive Cancer Center, School of Medicine, University of California, Davis, Sacramento, CA 95817, USA*

*Corresponding authors.

E-mail addresses: wangjj87@mail.sysu.edu.cn (Junjian Wang), hwzchen@ucdavis.edu (Hong-Wu Chen), jieh2015@yahoo.com (Jie Huang).

KEY WORDS

TIGAR;
NSD2;
NRF2;
Metabolism;
Oxidative stress;
Epigenetic
  reprogramming;
Therapeutic resistance;
Redox homeostasis

Abstract Metabolic and epigenetic reprogramming play important roles in cancer therapeutic resistance. However, their interplays are poorly understood. We report here that elevated TIGAR (TP53-induced glycolysis and apoptosis regulator), an antioxidant and glucose metabolic regulator and a target of oncogenic histone methyltransferase NSD2 (nuclear receptor binding SET domain protein 2), is mainly localized in the nucleus of therapeutic resistant tumor cells where it stimulates NSD2 expression and elevates global H3K36me2 mark. Mechanistically, TIGAR directly interacts with the antioxidant master regulator NRF2 and facilitates chromatin recruitment of NRF2, H3K4me3 methylase MLL1 and elongating Pol-II to stimulate the expression of both new (NSD2) and established (*NQO1/2*, *PRDX1* and *GSTM4*) targets of *NRF2*, independent of its enzymatic activity. Nuclear TIGAR confers cancer cell resistance to chemotherapy and hormonal therapy *in vitro* and in tumors through effective maintenance of redox homeostasis. In addition, nuclear accumulation of TIGAR is positively associated with NSD2 expression in clinical tumors and strongly correlated with poor survival. These findings define a nuclear TIGAR-mediated epigenetic autoregulatory loop in redox rebalance for tumor therapeutic resistance.

1. Introduction

Cancer therapeutic resistance often involves epigenetic and metabolic reprogramming[1−4]. For instance, NSD2, also known as MMSET, preferentially dimethylates H3K36 and is overexpressed in a subset of multiple myeloma and many types of solid tumors including breast, prostate and lung cancers[1,5−9]. Work from us and others has demonstrated that NSD2 overexpression promotes cancer cell survival and drives endocrine resistance while *NSD2* silencing sensitizes cancer cells to chemotherapy[1,5,7,10]. One major mechanism of aberrant NSD2 functions is to mediate epigenetic reprogramming to de-regulate the expression of key glucose metabolic enzymes (HK2, G6PD and TIGAR) in reprograming tumor glucose metabolism[1,11]. However, the mechanism that drives NSD2 overexpression in therapeutic resistant cancer cells remains unclear.

TIGAR (TP53-induced glycolysis and apoptosis regulator) functions as a fructose-2,6-bisphosphatase (F2,6bPase) to redirect glucose carbon flux from glycolysis to the pentose phosphate pathway (PPP)[12]. Enhanced PPP can promote the production of NADPH to strengthen cellular antioxidant defense and protect cells from ROS-associated cell damage and apoptosis in neurons, skeletal muscle and oocytes[13−15]. In addition, TIGAR has been reported to be involved in different stages of cancer progression, including development and metastasis[16−18]. High levels of TIGAR were observed in multiple types of cancers and correlated strongly with poor survival of patients in chronic lymphocytic leukemia, ovarian cancer, lung cancer and nasopharyngeal carcinoma[9,17,19−21]. Moreover, several studies showed that TIGAR was associated with cancer therapy resistance. The expression of TIGAR was up-regulated in cancer cells treated with chemotherapy, ionizing radiation or targeted therapeutics and TIGAR silencing sensitized cells to the therapies[9,18,22−24]. In tamoxifen resistant breast cancer cells, NSD2 is recruited to the promoter-proximal region to stimulate TIGAR expression *via* its methylase activity[1]. Although initially identified as a P53 target, TIGAR's overexpression is often uncoupled from P53 and displays different biological functions in a context-dependent manner. In a KRAS-driven pancreatic ductal adenocarcinoma model, TIGAR plays distinct functions in different stages of cancer development and progression *via* controlling cellular ROS level[25]. As a glycolysis modulator, TIGAR was shown to localize in cytoplasm and associate with mitochondria in complex with the hexokinase HK2 in response to hypoxia[26]. TIGAR can also translocate into mitochondria and promote mitochondrial functions *via* SIRT1 (sirtuin 1)-PGC1α (PPARG coactivator 1 alpha) pathway[14]. Interestingly, the increased nuclear localization of TIGAR has also been observed in chemotherapy drug or hypoxia treated liver cancer cells and in metastatic lung cancer cells[17,27]. However, the function of nuclear TIGAR remained unknown.

The transcription factor NF-E2-related factor-2 (*NRF2*) is a master activator of genes for cell antioxidant response[28,29]. In normal cells without oxidative stress, *NRF2* is kept in the cytoplasm at a low level by KEAP1 for proteasome degradation. Under oxidative and other stresses, the ubiquitin ligase activity of KEAP1 is inactivated, allowing *NRF2* to accumulate and bind as a heterodimer with so-called small MAF proteins binds to the antioxidant response element (ARE) at target genes, such as *NQO1*, *HO1* and *GCLM* in stimulation of their expression[28,30]. However, in cancer cells and tumors, NRF2 is often constitutively activated due to the loss of KEAP1 function, induction by *KRAS* and *MYC* oncogenes, or other poorly defined mechanisms[28,29]. *NRF2* can directly stimulate the expression of PPP and other NADPH generating enzymes in maintenance of redox homeostasis in tumorigenesis and resistance to cancer therapeutics[28,30,31]. Thus, NRF2 appears to display similar functions to those of TIGAR in cancers[25], suggesting that NRF2 and TIGAR may be coordinated in driving cancer progression.

In this study, we demonstrate that TIGAR can act as a transcriptional regulator. Nuclear accumulation of TIGAR was markedly elevated in therapeutic resistant tumor cells and strongly correlated with poor survival in therapeutics-treated patients. Nuclear TIGAR interacts with NRF2 and facilitates NRF2 translocation to the nucleus to activate the expression of NSD2 and the antioxidant program in conferring cancer therapeutic resistance. We thus uncovered a novel, nuclear function of TIGAR in mediating a positive feedback loop involving TIGAR, NRF2 and NSD2 in reprogramming of epigenetics and redox homeostasis for cancer therapeutic resistance.

2. Materials and methods

2.1. Cell culture and transfection

Human breast cancer cell lines MCF-7 and T47D, non-small-cell lung carcinoma (NSCLC) cell line A549, lung carcinoid cell line H727, and embryonic kidney cell line 293T were obtained from American Type Culture Collection (ATCC, USA). MCF-7 and 293T cells were cultured in DMEM supplemented with 10% fetal bovine serum (FBS). T47D, A549 and H727 cells were cultured in RPMI1640 supplemented with 10% fetal bovine serum (FBS). The tamoxifen resistant (TamR) sublines MCF-7 TamR and T47D TamR and radioresistant subline MCF-7 RadR (MCF-7/C6) cells were generated and cultured as described previously[1,32]. The doxorubicin resistant (DoxR) sublines A549 DoxR cells were generated by maintaining the parental cells in medium containing 5−50 nmol/L doxorubicin for over 6 months. All cell culture media were supplemented with 100 U/mL penicillin and 100 μg/mL streptomycin (Gibco, Grand Island, NY, USA). Cells were grown at 37 °C in 5% CO_2 incubators and transfected using DharmaFECT1 for siRNA knockdown.

2.2. Antibodies and chemicals

Antibodies against the following proteins/epitopes were used with the sources and dilution for Western blotting indicated: NSD2 [Abcam, ab75359 (29D1); 1:2000]; TIGAR (Abcam; ab37910; 1:2000; Santa cruz; sc-166291; 1:500); HK2 (Cell signaling; #2867; 1:2000); G6PD (Abcam; ab133525; 1:2000); GAPDH (Cell signaling; #2118; 1:4000); β-actin (Santa cruz; sc-47778; 1:2000); NRF2 [Santa cruz (H-300); sc-13032; 1:500]; KEAP1 (Santa cruz; sc-15246; 1:500); CDC6 (Santa cruz; sc-9964; 1:500); tubulin (Santa cruz; sc-5286; 1:2000); cleaved-PARP1 (Cell signaling; #9542; 1:1000); cleaved-caspase7 (Cell signaling; #9491; 1:1000); H3K36me1 (Abcam; ab9048; 1:2000); H3K36me2 (Active Motif; #39255; 1:2000); H3K36me3 (Abcam; ab9050; 1:2000); H3K9me3 (Abcam; ab8898; 1:2000); H3K27me3 (Abcam; ab6002; 1:2000); H3K4me3 (Abcam; ab8580; 1:2000); H3 (Active Motif; #39163; 1:2000); V5-tag (Abcam; ab27671; 1:2000). Antibodies used for ChIP assays are the following: NSD2 (rabbit antiserum, as described in Ref. 7; TIGAR (Abcam, ab37910, Lot. GR16129-1); NRF2 [Santa cruz (H-300); sc-13032]; H3K36me2 (Active Motif; #39255); H3K27ac (abcam; ab4729), H3K4me3 (Abcam; ab8580), H3 (Active Motif; #39163), MLL (EMD Millipore; clone 9-12; #05-765), RNA polymerase II (Santa cruz; sc-899), pSer2-CTD of Pol-II (Active Motif; #61083), pSer5-CTD of Pol-II (Active Motif; #39749), MAFF (Boster, A07784-2), and MAFG (Boster, A04636-2). Sources for chemicals are as follows: *tert*-butylhydroquinone (tBHQ, Sigma, #112941), hydrogen peroxide solution (Sigma, H1009), 4-hydroxytamoxifen (Sigma, H7904), doxorubicin hydrochloride (Dox, TargetMol, T1020). Other chemicals are from Sigma (St. Louis, MO, USA) unless indicated otherwise.

2.3. Generation of lentiviruses and TIGAR stable expression subline cells

V5-tagged TIGAR (WT) lenti-vector in pLX304 was from DNASU (https://dnasu.org). TIGAR-TM (triple-mutation, H11A/E102A/H198A)[12], which lost the ability to hydrolyze Fru-2,6-P2, kindly provided by Dr. Karen Vousden (The Beatson Institute, UK) was PCR amplified and inserted into a modified version of pLX304 and the mutations were confirmed by sequencing.

Nuclear localization signal (NLS) sequence (3X)- and V5-tagged TIGAR was generated in the modified pLX304 vector with the NLS sequence tagged at the C-terminus TIGAR and the V5 sequence tagged at the N-terminus. Lentiviruses were produced in 293T cells after co-transfection of the above lentivirus vector, psPAX2 and pMD2.G into cells in 10 cm dishes, as described[33]. To generate TIGAR-overexpressing A549 cell sublines, A549 cells were infected for 6 h, in the presence of polybrene, with the above lentivirus. Infected cells were selected with Blasticidin (10 μg/mL, InvivoGen, USA) for 4−6 weeks. Individual blasticidin-resistant clones were isolated, expanded and examined for ectopic TIGAR expression by immunoblotting. Clones homogeneously expressing TIGAR were maintained in medium containing 10 μg/mL blasticidin.

2.4. Apoptosis, cell growth, qRT-PCR, immunoblotting and ChIP assay

Cell apoptosis and growth assays were performed as previously described[7,8]. Gene expression analyzed by qRT-PCR, immunoblotting and ChIP assay was performed as previously described[7,8]. Primers are listed in the Supporting Information Table S1.

2.5. Assays for NADPH/$NADP^+$ ratio, G6PD activity and ROS level

Different times after the indicated treatments, cells were washed with PBS, scraped and harvested. $NADP^+$/NADPH ratios were measured with $NADP^+$/NADPH quantification kit (BioVision, USA) and G6PD activity was measured with Glucose-6-Phosphate Dehydrogenase Activity Assay Kit (BioVision, USA) following their corresponding instruction. ROS levels were analyzed as previously described[1,33].

2.6. siRNAs

siRNAs for gene knockdown were purchased from Dharmacon (Thermo, USA) and used following the manufacture's protocol. The siRNA target sequences for each gene are as follow: *NSD2*#1, AGGGAUCGGAAGAGUCUUCAA; *NSD2*#2, GCACGCUACAACACCAAGU; *TIGAR*#1, GCAGCAGCUGCUGGUAUAU; *TIGAR*#2, UUAGCAGCCAGUGUCUUAG; *TIGAR*#3, GCAUGGAGAAACAAGATTTAA; *HK2*#1, CCAAAGACAUCUCAGACAUUG; *HK2*#2, GCAGAAGGUUGACCAGUAUCU; *Nrf2*#1, AUAAUUGUCAACUUCUGUCAGUUUG; *Nrf2*#2, AAUGAGUUCACUGUCAACUGGUUGG; Control, CAGUCGCGUUUGCGACUGG.

2.7. Co-immunoprecipitation (Co-IP)

Cells were lysed in RIPA lysis buffer [Tris-HCl, 50 mmol/L, pH 7.4; Nonidet P-40 (NP-40), 1%; deoxycholate-Na, 0.25%; NaCl, 120 mmol/L; EDTA, 1 mmol/L; 1% glycerol] freshly supplemented with 1 mmol/L PMSF, protease inhibitor cocktail from Roche, 1 mmol/L NaF and 1 mmol/L $NaVO_3$ on ice for 30 min. Lysates were centrifuged at 4 °C for 10 min at 10,000 × *g*. The protein concentration was measured and normalized. 5 mg protein (10 mg/mL) was precleared with 60 μL protein A/G (1:1) agarose beads (Roche, USA) at 4 °C for 1 h, then incubated with 3 μg primary antibody or normal rabbit IgG as a control at 4 °C overnight and subsequently with 50 μL protein A/G agarose beads for 2 h at 4 °C. Beads were washed 3 times with lysis buffer. The immunoprecipitates were boiled in 50 μL SDS sample buffer for

10 min, and half of the sample volume was analyzed by immunoblotting.

2.8.   GST pull-down assay

GST pull-down was performed as previously described[7]. TIGAR cDNA (WT or the TM mutant) were PCR amplified and inserted into pGEX-KG vector at BamHI and XbaI sites and the inserted DNA fragments were sequenced. His-tagged NRF2 in pET28b (+) were described in Kim's report[34], or made by inserting the PCR product for aa 534−605 of NRF2 into pET28b (+) at XhoI and BamHI sites. His-p97/VCP was described before[35].

2.9.   Reporter gene assay

Transient transfection and reporter gene assays were performed as previously described[7]. HEK293T cells were transfected with NQO-1-ARE-luciferase reporter plasmid, expression plasmid for NRF2 and TIGAR in pLX304 vector from DNASU (https://dnasu.org), and pCMV-beta-Gal was used as internal control.

2.10.   Immunofluorescence microscopy

Cells on the coverslips were fixed with 4% paraformaldehyde for 10 min and permeated by treatment with blocking buffer (1 × PBS plus 10% normal goat serum) containing 0.25% Triton X-100 for 30 min. Cells were the incubated with anti-TIGAR antibody (rabbit, Abcam; ab37910; mouse, Santa cruz; sc-166291), anti-NRF2 antibody (rabbit, Proteintech; 16396-1-AP; rabbit, Gene-Tex; GTX103322) or anti-V5-tag (mouse monoclonal, Abcam; ab27671), used at 1:500. Cell nuclei were stained with DAPI. Alexa-488 conjugated anti-rabbit IgG (Molecular Probe) and Alexa-488 conjugated anti-mouse IgG (Molecular Probe) were used at 1:1000 as secondary antibodies. Images were captured in a Zeiss LSM780 laser-scanning microscope (Zeiss, Germany) with a Plan-Apochromat 40 × oil immersion objective. Images were processed using the tool in the LSM 780 Meta ZEN 2011 software package.

2.11.   Immunohistochemistry (IHC), patient tumor specimens, and statistics analysis

IHC was performed as previously described[7,8]. Sections of tissue microarrays (TMAs) were incubated with anti-NSD2 monoclonal antibody (Abcam, 29D1) or anti-TIGAR antibody (Abcam37910, Lot. GR16129-1), at 1:50 and 1:100 dilutions respectively, overnight at 4 °C, followed by incubations with biotinylated secondary antibody and the ABC reagents in the Vectastain Elite Kit, visualized by staining with diaminobenzidine chromogen solution and followed by counterstaining with hematoxylin. TMAs contained specimens from about 450 cases of informative breast cancer patient who were subsequently treated with adjuvant tamoxinfen therapy. All primary invasive breast cancers used in this study were from the Manitoba Breast Tumor Bank (MBTB, CancerCare Manitoba and University of Manitoba)[36]. MBTB embraces the policies and operating protocols of the Canadian Tumor Repository Network and operates with approval from the Research Ethics Board of the Faculty of Medicine, University of Manitoba (Canada). The histopathology assessment of the MBTB biospecimens, the cohort characteristics, ERα-positive status determination, and sample selection for tissue microarray (TMA) construction are described before[37]. A total of 450 cases were represented on the original TMAs. The tumor numbers (n) analyzed for some markers, however, were less than 450, due to exhaustion of some tumor cores from previous uses. The current cohort characteristics are progesterone receptor (PR)-positive (>20 fmol/mg protein), 77.7% (261/336); PR-negative, 37.5% (126/336); low-grade, 27.7% (93/336); intermediate-grade, 61.6% (207/336); high-grade, 10.7% (36/336); tumor size <2.5 cm, 55.5% (187/337); tumor size ≥2.5 cm, 44.5% (150/337); age <50 years, 6.9% (23/335); age >50 years, 93.1% (312/335); node-negative, 49.6% (164/331); node-positive, 50.5% (167/331). The median follow-up was 99 months (range 9−217 months). The TMA section was scored negative if <1% of the breast epithelial cells displayed any staining and scored positive if >5% of the cells displayed staining in the nucleus with moderate to high intensity. High TIGAR expression by immunostaining was defined as >10% and low was 0−10%. Relationships in immunostaining among groups were analyzed with the χ^2 test. Other statistical analysis was performed as previously described[37].

2.12.   Analysis of tumor TIGAR mRNA expression association with clinical outcome

The Kaplan−Meier estimates were used to compute the survival curves. Kaplan−Meier curves were obtained for relapse-free survival times of breast cancer patients ($n = 665$) who received tamoxifen only and lung cancer patients, and with tumors stratified by TIGAR expression levels, using an online survival analysis tool (http://kmplot.com), as described[1,38]. Statistical significance was determined by the log-rank test.

2.13.   Xenograft tumor models

BALB/c nu/nu athymic mice (4 weeks old) were purchased from GemPharmatech, Nanjing, China. Briefly, 5×10^6 A549 or A549-TIGAR-NLS cells were suspended in 100 μL PBS/Matrigel (1:1) and subcutaneously injected into male BALB/c nu/nu athymic mice. When the tumor volume was approximately 80 mm^3, the mice were randomly grouped ($n = 7$ mice per group) and received vehicle or doxorubicin (intraperitoneally (i.p.); 4 mg/kg per five days). Tumor growth was monitored every 3 days by calipers with volume calculated using Eq. (1):

$$V = \pi \times \left(\text{Length} \times \text{Width}^2\right)/6 \qquad (1)$$

The mice were sacrificed at the end of the studies. Tumors were harvested, weighted and subjected to further use. All animal care and experiments were approved by the Institutional Animal Care and Use Committee of Sun Yat-sen University, Guangzhou, China.

2.14.   Statistical analysis

Cell culture-based experiments were performed three times or more unless indicated otherwise. The data are presented as mean values ± standard deviation (SD) from three independent experiments. Statistics analysis was performed using two-tailed Student's t tests to compare means. $P < 0.05$ was considered significant. Patient survival curves were generated using the Kaplan−Meier method, taking into account censored data. The curves were compared using the log-rank test (Mantel-Cox)[37]. Pearson's χ^2 test was used to determine the immunostaining association between NSD2 and nuclear TIGAR.

3. Results

3.1. TIGAR stimulates NSD2 overexpression and global histone H3K36 methylation in therapeutic resistant cancer cells

Our previous study demonstrated that TIGAR was strongly up-regulated by NSD2 in the therapeutic resistant cancer cells[1]. This prompted us to examine whether TIGAR is involved in the resistance. First, we analyzed the effects of TIGAR silencing on cancer cell survival and found that TIGAR knockdown strongly induced apoptosis in therapeutic resistant cancer cells including MCF-7 TamR (tamoxifen resistance) and MCF-7 RadR (ionizing radiation-resistance) (Supporting Information Fig. S1). Interestingly, TIGAR silencing resulted in more significant inhibition of growth in therapeutic resistant MCF-7 TamR and MCF-7 RadR cells than in the therapeutic-sensitive parental cells (Fig. 1A and B). Surprisingly, we observed that knockdown of TIGAR resulted in a dramatic decrease of NSD2 protein and mRNA expression preferentially in the therapeutic resistant cancer cells (Fig. 1C and D). In the tamoxifen-sensitive cells the inhibition was marginal (Fig. 1C and D). Moreover, consistent with the inhibition of NSD2 expression, TIGAR silencing in TamR cells markedly decreased the NSD2 methylase activity-associated global H3K36me2 level but not that of other histone H3 marks (Fig. 1E). Together, these results suggest that in therapeutic resistant cells, elevated TIGAR is required for the overexpression of NSD2 and NSD2-associated histone hypermethylation at H3K36.
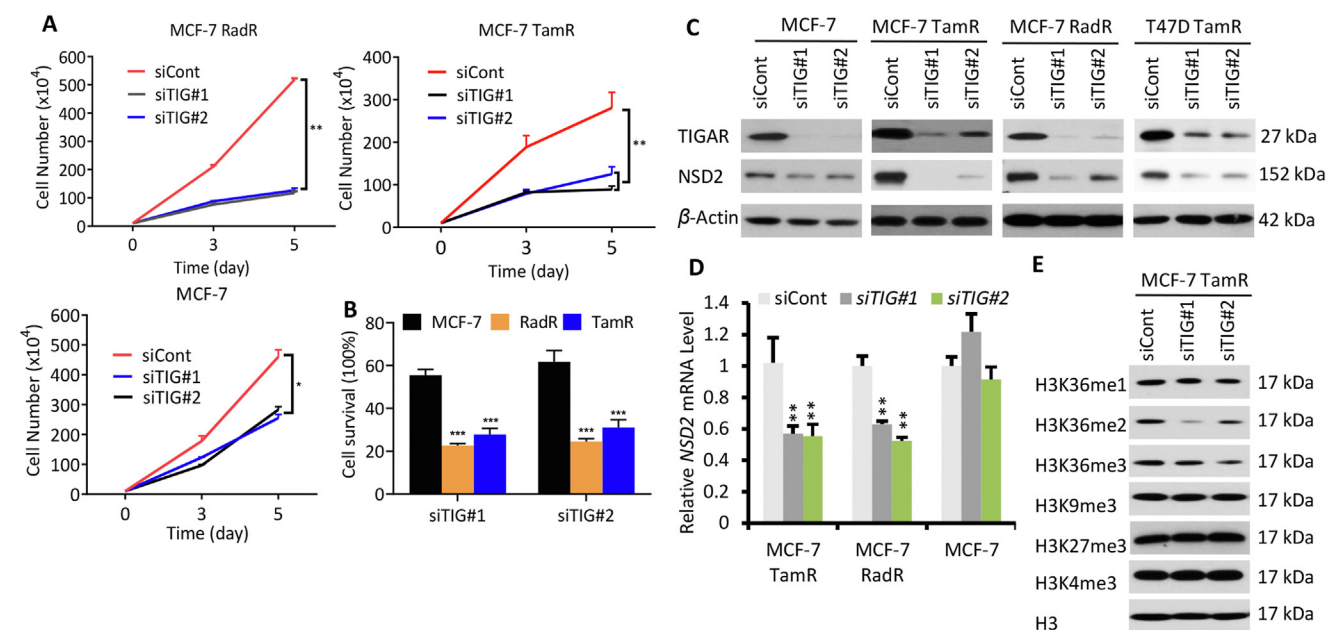
3.2. TIGAR is localized in the nucleus of therapeutic resistant cancer cells

Our unexpected observation of the strong impacts of TIGAR knockdown on NSD2 expression and activity prompted us to examine the possibility of TIGAR function as a gene expression regulator. First, we examined the subcellular localization of TIGAR in the cancer cells. Immunofluorescence (IF) analysis shows that a major proportion of endogenous TIGAR protein was localized in the nucleus of TamR cells, RadR cells and DoxR cells (Fig. 2A and Supporting Information Fig. S2). Immunoblotting analysis of fractionated cell extracts also demonstrated that a high proportion of TIGAR was localized in the nuclei of the resistant cells (Fig. 2B). Moreover, ectopic expression of V5-tagged wild type (V5-TIGAR) was mainly localized in the nuclei of TamR cells. In contrast, V5-tagged G6PD protein was localized in the cytoplasm (Fig. 2C). Interestingly, three-point mutations that inactivate TIGAR's enzymatic activity[12] (V5-TIGAR-TM) did not affect TIGAR protein nuclear localization, suggesting that nuclear localization of TIGAR protein is independent of TIGAR enzymatic activity. To further verify TIGAR nuclear localization, we performed IF analysis using a different anti-TIGAR antibody. The results also show that TIGAR was mainly localized in the nucleus and that *TIGAR* siRNA dramatically decreased TIGAR level in the nucleus (Fig. 2D). Together, these results strongly suggest that TIGAR is mainly localized in the nuclei of therapeutic resistant tumor cells and may function as a gene expression regulator.

Figure 1 TIGAR mediates NSD2 overexpression and global histone methylation in therapeutic resistant cancer cells. (A) The indicated cells were transfected with *TIGAR* or control siRNA, after the indicated time points, viable cells were counted. (B) The indicated cells were transfected with *TIGAR* or control siRNA, after 5 days, viable cells were counted. Cell survival rate was calculated as a percentage of the viable cells in *TIGAR* siRNA *versus* control siRNA treated group. (C) The indicated cells were transfected with *TIGAR* or control siRNA. Three days later, cells were harvested for immunoblotting analysis. (D) MCF-7-TamR, MCF-7 RadR and MCF-7 cells were transfected with *TIGAR* or control siRNA. Two days later, cells were harvested for analysis of relative *NSD2* mRNA levels by qRT-PCR. (E) MCF-7-TamR cells were transfected with *TIGAR* or control siRNA. Three days later, cells were harvested for immunoblotting with antibodies against total or modified histone H3. Results shown are representative of at least three independent experiments. The data are presented as the mean $\pm$ SD of triplicate of each sample ($n = 3$; $*P < 0.05$, $**P<0.01$, $***P<0.001$).
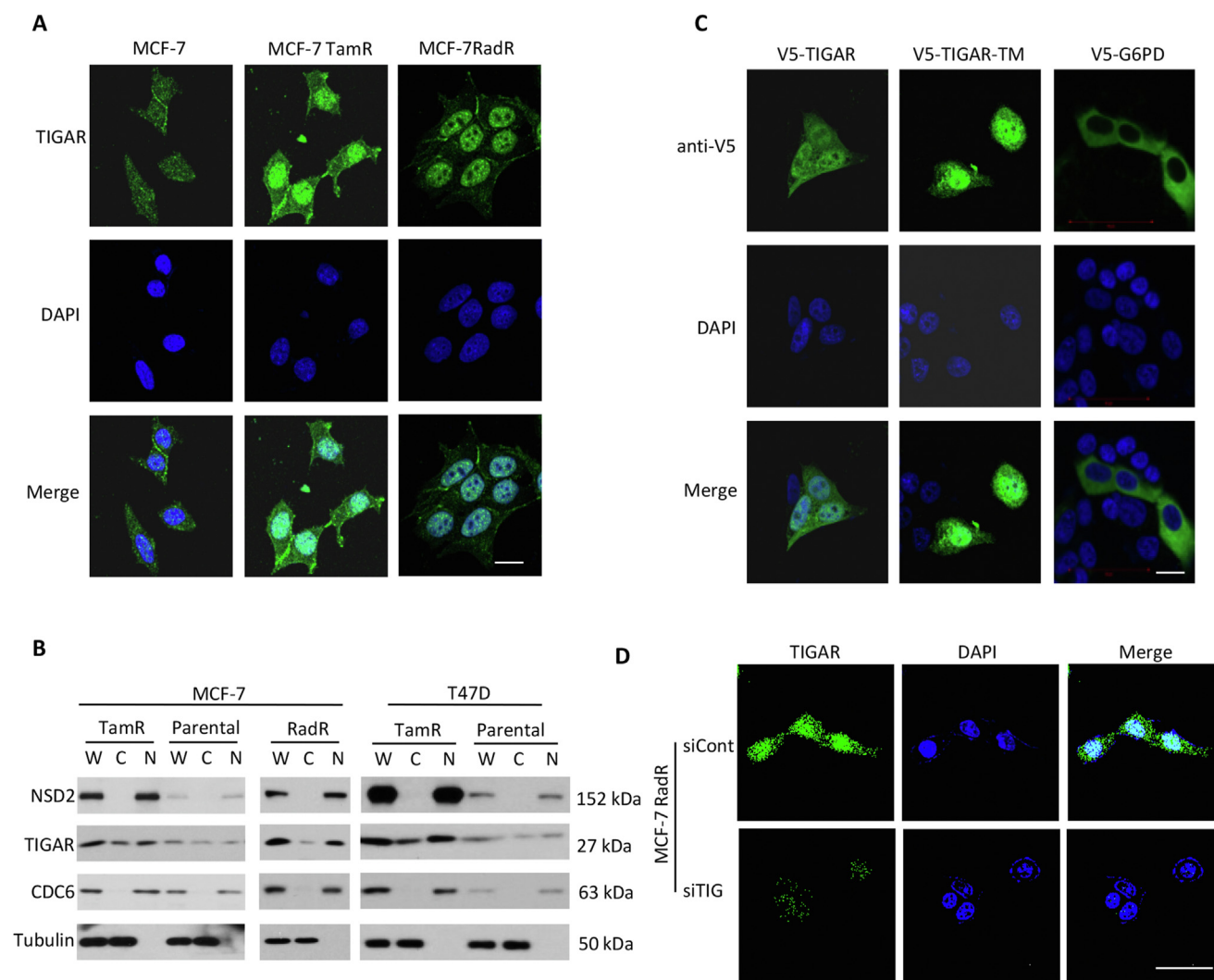
Figure 2 TIGAR is translocated into the nucleus of therapeutic resistant cancer cells. (A) Cellular localization of endogenous TIGAR protein in indicated cells was examined by IF confocal microscopy (original magnification, 400 ×). Cells were immunostained with anti-TIGAR antibody (green, ab37910). The nucleus is marked with DAPI (blue). The scale bar represents 10 μm. (B) Immunoblotting of whole cell lyates (W), cytoplasmic (C) or nuclear (N) extractions from indicated cells. (C) MCF-7 TamR cells, transfected with V5-TIGAR (WT: wild type and TM: triple mutation) and V5-G6PD protein expressing PLX304 plasmid, were examined by IF confocal microscopy (original magnification: 400 ×). Cells were immunostained with anti-V5 (green). The nucleus is stained with DAPI (blue). The scale bar represents 10 μm. (D) MCF-7 RadR cells were transfected with TIGAR or control siRNA. Three days later, cellular localization of endogenous TIGAR protein in indicated cells was examined by IF confocal microscopy (original magnification, 400 ×). Cells were immunostained with anti-TIGAR antibody (green, sc-166291). The nucleus was stained with DAPI (blue). The scale bar represents 20 μm.

3.3. Nuclear TIGAR acts as a novel NRF2 coactivator in stimulation of NSD2 expression and an antioxidant program

To determine whether nuclear TIGAR directly controls *NSD2* gene expression, we performed ChIP with anti-TIGAR antibody to detect potential TIGAR association with a chromatin region with qPCR primer sets designed to scan a 10 kb region of *NSD2* gene. Indeed, our ChIP analysis demonstrated that *TIGAR* specifically occupied a region centered approximately 1 kb upstream of *NSD2* transcriptional start site (TSS). Interestingly, the TIGAR occupancy at the *NSD2* promoter region was significantly increased by tamoxifen in the TamR cells but not in the tamoxifen-sensitive cells (Fig. 3A). Upon examination of possible transcription factor binding sites at the *TIGAR* binding region, we identified two

putative sites for transcription factors *NRF2*, the primary regulator of cellular antioxidant program (Supporting Information Fig. S3A). Our further ChIP demonstrated that *NRF2* indeed bound to the same region as *TIGAR* and that its binding, like that of *TIGAR*, was also increased by tamoxifen (Fig. 3B). Next, to examine the function of *TIGAR* at *NSD2* promoter, we knocked down *TIGAR* and then performed ChIP. Results show that *TIGAR* knockdown strongly diminished the occupancy by *NRF2* at *NSD2* promoter (Fig. 3C and Fig. S3B). Thus, high levels of *TIGAR* were crucial for recruitment of *NRF2*. Similar *TIGAR* knockdown and ChIP analysis demonstrated that *TIGAR* mediates the recruitment of histone methylase MLL1, the NRF2 heterodimerization partner MAFF and MAFG, and the deposition of activating histone mark H3K4me3 and H3K36me2 at *NSD2* promoter. Moreover, *TIGAR*

was also important for recruitment of transcriptional elongation-competent RNA polymerase II complex at *NSD2* promoter as *TIGAR* suppression significantly decreased the occupancy of phospho-Ser2 form of Pol-II CTD (Fig. 3C and Fig. S3E). These results suggest that nuclear TIGAR plays an important role in facilitation of *NRF2* activation of *NSD2* gene expression in the therapeutic resistant cells.

Next, to examine whether *TIGAR* functions as a novel coactivator of *NRF2*, we performed an antioxidant response element (ARE)-driven reporter assay. Our results show that co-expression of *TIGAR* strongly enhanced *NRF2*-mediated transactivation (Fig. 3D). Consistently, *TIGAR* also induced *NSD2* promoter-driven luciferase activity (Fig. S3C). To address whether the fructose-2,6-bisphosphatase activity of TIGAR is involved, we performed the reporter assay with the mutant TIGAR that contains three point mutations (TIGAR TM) that eliminates its enzymatic activity as previously reported[1]. Interestingly, the mutant TIGAR displayed a coactivator activity similar to that of the wild type TIGAR (Fig. 3D). Further supporting that *TIGAR* is a novel coactivator of *NRF2* and that *NSD2* is a novel target of *NRF2*, we found that, in cells treated with an *NRF2* activator compound tBHQ, *TIGAR* suppression strongly inhibited tBHQ induction of *NSD2* as well as a number of previously established *NRF2* target genes such as *NQO2*, *PRDX1*, *GCLM* and *GSTM4*[39] (Fig. 3E). Furthermore, ChIP analysis with the TamR cells demonstrated that *NRF2* is critical for *TIGAR* occupancy and the high level of H3K4me3 mark at *NSD2* promoter (Fig. S3D). As it might be expected, knockdown of NRF2 and TIGAR strongly inhibited the expression of NSD2 and its targets HK2, G6PD and TIGAR in the TamR and A549 cells (Fig. 3F, G, Fig. S3F and S3G). *TIGAR* knockdown also decreased NRF2 protein level (Fig. S3H), whereas the knockdown did not change the expression of KEAP1. Moreover, similar to the effects seen with TIGAR suppression, a dramatic rise of ROS and cell death and a decrease of NADPH were observed in the TamR cells with NRF2 knockdown (Fig. S3I). Together, these results strongly suggest that nuclear TIGAR can act as a transcriptional coactivator of NRF2 to facilitate NRF2 recruitment to target gene *NSD2* and *NRF2*-mediated activation of antioxidant program.

3.4. TIGAR physically interacts with NRF2 and promotes NRF2 nuclear translocation

It is well established that NRF2, a master regulator of antioxidant defenses, translocates to the nucleus upon activation by oxidative stress. Since our study identified TIGAR acting as a novel coactivator of NRF2, we next examined whether nuclear TIGAR is also involved in antioxidant defenses. Employing IF analysis, we indeed found that NRF2 activating compound tBHQ significantly increased nuclear localization of TIGAR in cancer cells (Supporting Information Fig. S4A). We also observed that TIGAR silencing decreased the nuclear NRF2 signal induced by H_2O_2 (Fig. 4A and Fig. S4B). To further examine whether TIGAR is involved in NRF2 translocating into nucleus, we expressed TIGAR with a nuclear localization signal (NLS) sequence. IF analysis shows that V5-tagged TIGAR-NLS was exclusively expressed in the nucleus and strongly enhanced NRF2 accumulation in nucleus (Fig. 4B).

We next examined whether TIGAR and NRF2 physically interacted with each other in cancer cells. Reciprocal co-IP experiments show that endogenous TIGAR was indeed associated with NRF2 in TamR cells, and that NRF2 activator tBHQ

treatment enhanced the association (Fig. 4C and Fig. S4C). GST pull-down with purified proteins demonstrated that TIGAR directly interact with NRF2 and that the interaction is independent of TIGAR enzymatic activity (Fig. 4D, left). Furthermore, GST pull-down with different truncated fragments of NRF2 protein showed that the interaction appeared to be mediated by the C-terminal, Neh1−Neh3 region of NRF2 which contains a bZIP DNA binding and transactivation domains[39] (Fig. 4D, right). These results collectively suggest that nuclear TIGAR directly associated with NRF2 and promotes NRF2 location.

3.5. Nuclear TIGAR promotes cancer therapy resistance via stimulating redox balance

We next examined whether elevated TIGAR alone is sufficient to drive therapeutic resistance through NSD2 and redox homeostasis. Ectopic expression of TIGAR, which distributed to both the nucleus and cytoplasm, resulted in a robust suppression of Tam-induced ROS and a significant increase of G6PD activity, and strongly promoted the survival of Tam-sensitive cells (Supporting Information Fig. S5A). Employing V5-tagged TIGAR-NLS which exclusively expressed in the nucleus, we examined whether nuclear TIGAR possesses similar functions. Our results show that nuclear TIGAR strongly enhanced NSD2 and HK2 expression, suppressed Tam-induced ROS and cell death, and increased cellular G6PD activity (Fig. 5A). Consistent with the notion that the function of nuclear TIGAR−NSD2 axis is not restricted to TamR cells, in the lung cancer cells that were treated by either chemotherapy drug doxorubicin or H_2O_2, expression of nuclear TIGAR dramatically induced NSD2 and HK2 protein expression and G6PD activity and strongly decreased ROS and cell death (Fig. 5B). Moreover, knockdown of TIGAR in lung cancer cells resulted in a marked decrease of cell survival especially when the cells were treated with doxorubicin (Fig. 5C). Interestingly, the F2,6bPase-defective mutant of TIGAR when endowed with NLS displayed activities similar to those of the wild type TIGAR in *NSD2* gene expression and ROS rebalance (Fig. 5A−C). Moreover, nuclear TIGAR expression strongly stimulated the expression of *NSD2*, *HK2*, *G6PD*, *NQO1* and *PRDX1* (Fig. S5B).

We next evaluated the effect of nuclear TIGAR on tumor growth and chemotherapy resistance. As shown in Fig. 5D, expression of nuclear TIGAR strongly promoted the growth of A549 lung cancer xenograft tumors (black line *versus* blue line). More importantly, nuclear TIGAR-overexpressing tumors were statistically more resistant to doxorubicin treatment than the vector-control tumors (Fig. 5D, E, Fig. S5C, and S5D; yellow line *versus* red line). In addition, immunoblotting analysis of tumor tissues revealed that nuclear TIGAR overexpression markedly increased NSD2 expression and blocked doxorubicin induction of cleavage of caspase and PARP1, which are indicators of cell death in the xenograft tumors (Fig. 5F). These results together with the results shown above suggest that TIGAR localized in the nucleus can act as a potent transcriptional coactivator of NRF2 to stimulate the downstream targets, such as NSD2, effectively rebalance ROS and confer cancer chemotherapy resistance.

3.6. Nuclear TIGAR strongly correlates with NSD2 expression and patient poor survival

To address the clinical significance of our findings, we next performed IHC to examine TIGAR protein expression and its cellular localization in the same cohort of breast cancer tumor specimens
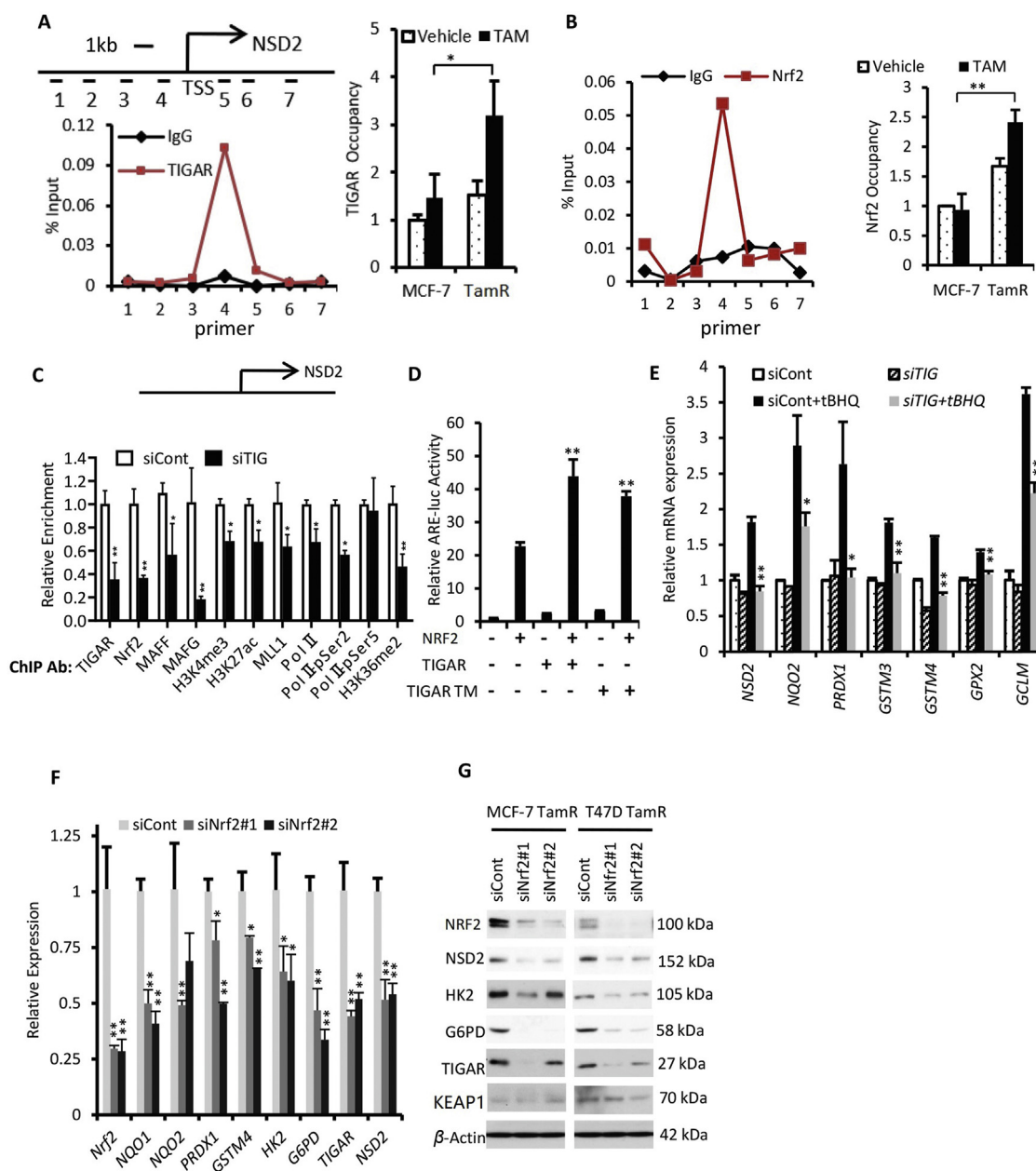
Figure 3 Nuclear TIGAR acts as a novel NRF2 coactivator for activation of NSD2 expression and the antioxidant program. (A) Left panels: top, schematics of NSD2 promoter region with indicated locations of primers used in ChIP assay. Bottom, ChIP analysis of TIGAR occupancy on NSD2 promoter region in Tam-treated, MCF-7-TamR cells. ChIP data are presented as a percentage of input signals. Right panel, relative TIGAR occupancy at the NSD2 promoter (primer 4 site) in MCF-7 parental and TamR cells treated with vehicle or tamoxifen (TAM, 1 µmol/L). (B) ChIP analysis of NRF2 occupancy at NSD2 promoter region in MCF-7-TamR cells (left) and at the NSD2 promoter site 4 in the indicated cells treated with vehicle or Tam (right). Results shown are representative of at least three independent experiments. (C) ChIP analysis of relative occupancy by NRF2, TIGAR, MLL1, RNA polymerase II (pol II), RNA pol II serine 2 phosphorylation (pol II-pSer2), RNA pol II serine 5 phosphorylation (pol II-pSer5) and H3K4me3 and H3K27ac marks at the NSD2 promoter site (primer 4) in MCF-7-TamR cells transfected with control or TIGAR siRNA. (D) Reporter gene assay with NQO-1-ARE-luciferase (right) and NSD2-promoter-luciferase (left) was performed by transfecting 293T cells with vectors for the NQO1-ARE-dependent *Firefly* luciferase reporter and indicated constructs for expressing NRF2, TIGAR, TIGAR TM (triple mutation). β-Gal construct was included as an internal control. (E) qRT-PCR analysis of indicated gene expression in MCF-7 cells transfected with siTIGAR or control siRNA, and treated with vehicle or tBHQ (50 µmol/L). (F) qRT-PCR analysis of indicated gene expression in MCF-7-TamR cells transfected with *NRF2* or control siRNA. (G) Whole cell lysates from MCF-7-TamR cells were prepared, and IP was performed with either anti-NRF2 antibody (top) or anti-TIGAR antibody (bottom) followed by IB with indicated antibodies. Results shown are representative of at least three independent experiments. The data are presented as the mean ± SD of triplicate of each sample ($n = 3$; *$P < 0.05$, **$P < 0.01$).
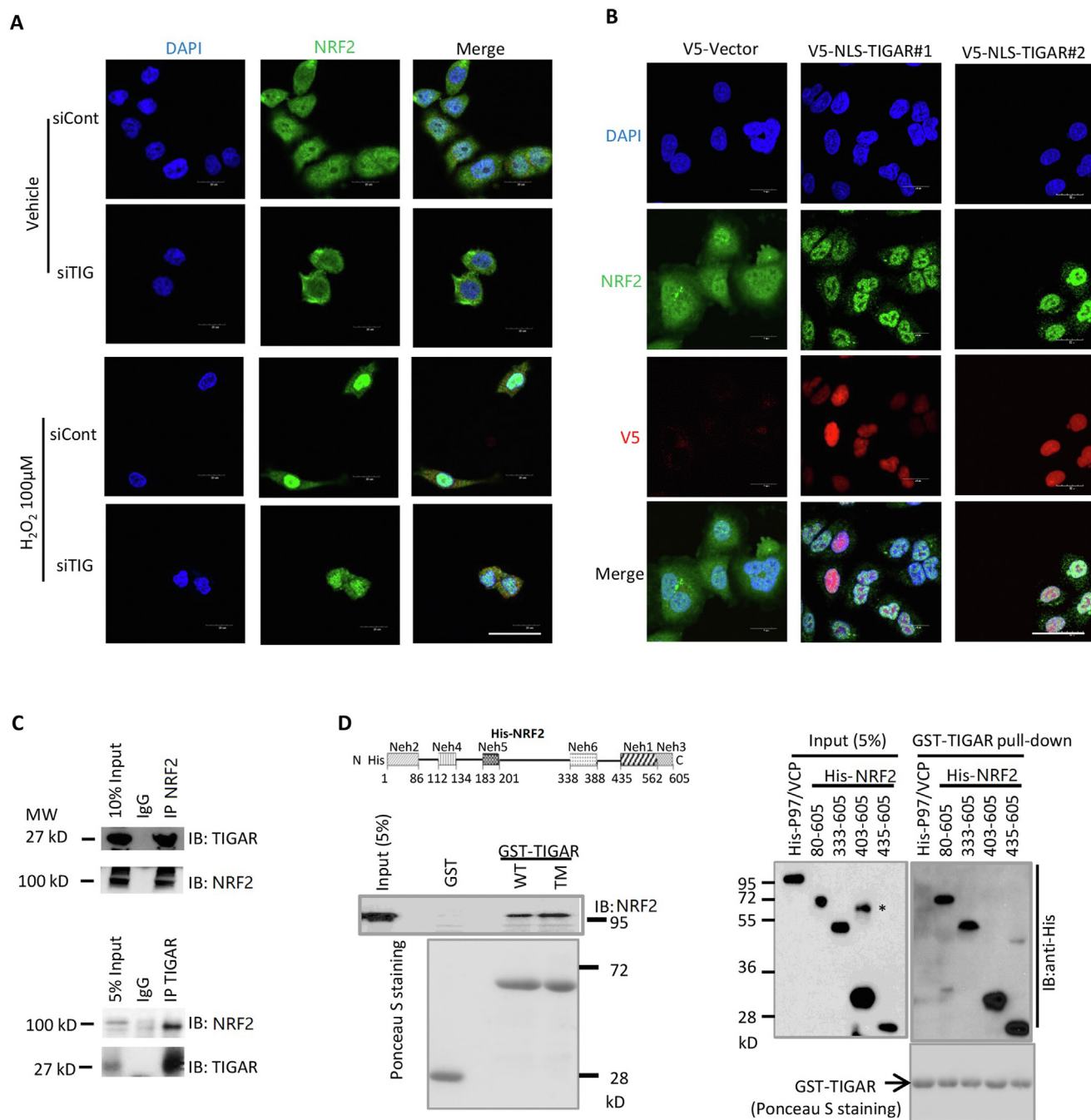
Figure 4 TIGAR physically interacts with NRF2 and promotes NRF2 nuclear translocation. (A) MCF-7 cells were transfected with *TIGAR* or control siRNA, after 3 days, cells treated with H_2O_2 or vehicle for another 6 h, subcellular localization of TIGAR were examined by IF confocal microscopy. Cells were immunostained with NRF2 antibody (green). The nucleus is stained with DAPI (blue). Merged images (Merge) are shown. The scale bar represents 20 μm. (B) Subcellular localization of V5 tagged TIGAR and NRF2 were examined by IF confocal microscopy in A549 vector control cells or nuclear localization signal (NLS) linked TIGAR overexpressing cells. Cells were immunostained with V5 antibody (red) and NRF2 antibody (green). The nucleus was stained with DAPI (blue). Merged images (Merge) are shown. The scale bar represents 20 μm. (C) Whole cell lysates from MCF-7-TamR cells were prepared, and IP was performed with either anti-NRF2 antibody (top) or anti-TIGAR antibody (bottom) followed by IB with indicated antibodies. (D) Top left, schematics of His-tagged human NRF2 protein with numbers indicating boundary amino acid number at the indicated domains. GST pulldown assays were performed with GST-wild (WT) or mutant (TM) TIGAR and full length His-tagged NRF2 or its deletion forms. His-p97/VCP was used as a negative control.

that we previously analyzed for NSD2[1]. Similar to other reports[40], TIGAR was detected in all tumor samples. In a cohort of 444 breast carcinoma specimens, a majority of the tumors showed varying levels of cytoplasmic expression (Fig. 6A, tumor #1, and data not shown). Interestingly, we observed that a high percentage (73.2%) of the tumors displayed nuclear TIGAR staining with
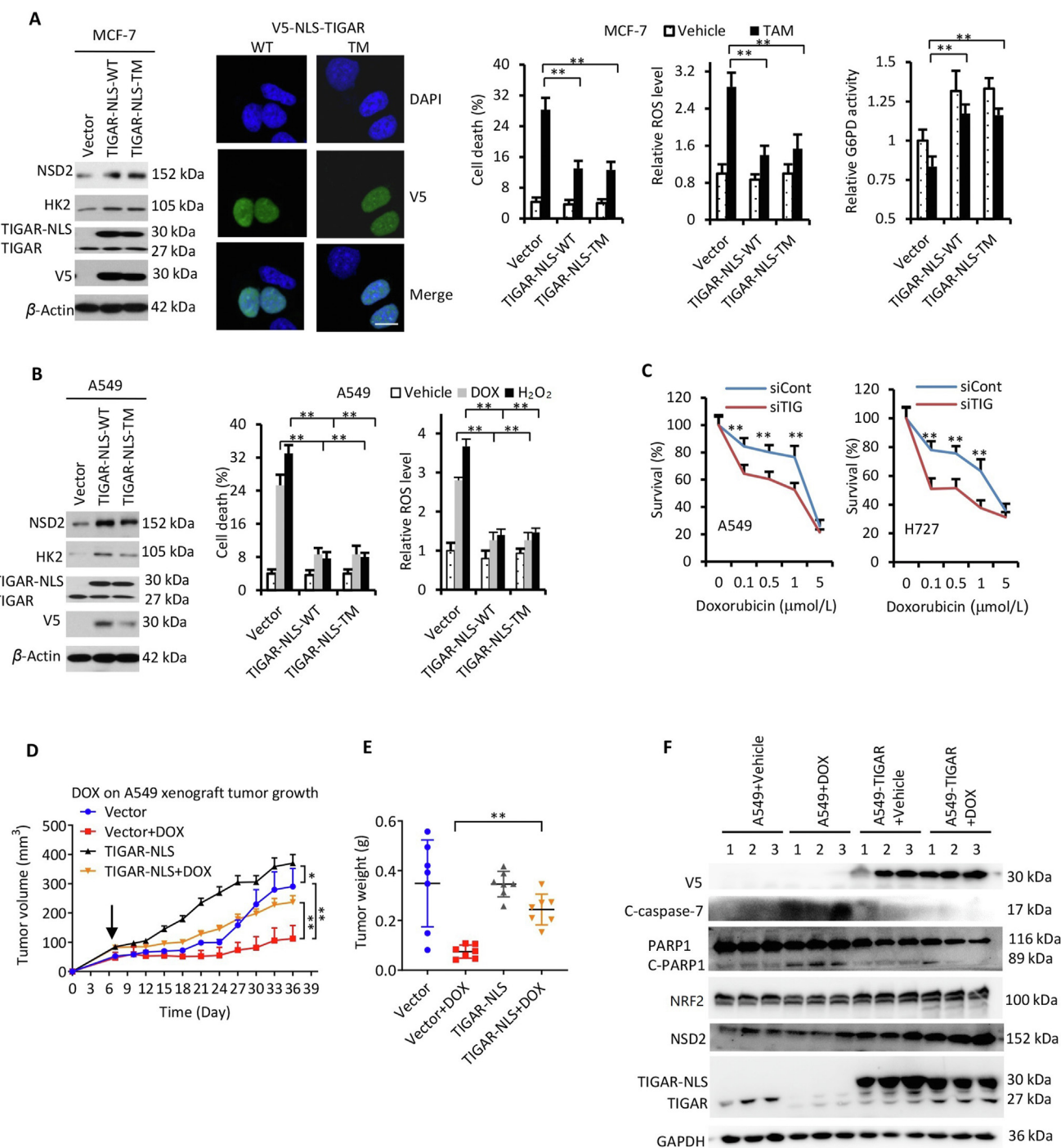
Figure 5 Nuclear TIGAR promotes cancer therapy resistance *via* stimulating redox balance. (A) MCF-7 cells were transduced with lentiviruses expressing V5-TIGAR-NLS (WT, wild type and TM, triple mutation), Three days later, TIGAR localization was examined by IF confocal microscopy (original magnification: $400 \times$), cells were immunostained with anti-V5 antibody (green). The nucleus is stained with DAPI (blue). The scale bar represents 10 μm. Cells were also analyzed by immunoblotting with indicated antibodies, or treated with tamoxifen or vehicle for another 24 h for analysis of ROS level, G6PD activity and for another 72 h for analysis of cell death. The data are presented as the mean ± SD of triplicates of each sample ($n = 3$; ** $P < 0.01$). (B) A549 cells were transduced with lentiviruses expressing V5-TIGAR-NLS. Three days later, cells were analyzed by immunoblotting with indicated antibodies, or treated with doxorubicin, H_2O_2 or vehicle for another 24 h for analysis of ROS level and for another 72 h for analysis of cell death. The data are presented as the mean ± SD of triplicates of each sample ($n = 3$; ** $P < 0.01$). (C) A549 and H727 lung cancer cells were transfected with TIGAR or control siRNA. Two days later, cells were treated with vehicle or doxorubicin for another 2 days, viable cells were counted. Results are representative of at least three independent experiments. The data are presented as the mean ± SD of triplicates of each sample ($n = 3$; ** $P < 0.01$). (D) and (E) Nude mice bearing the A549-TIGAR-NLS or A549-parental xenografts ($n = 7$ mice per group) received vehicle or doxorubicin [intraperitoneally (i.p.); 3 mg/kg per five days]. Black arrow indicates the starting point of administration. Mean tumor volume ± SEM and mean tumor weight ± SEM are shown (** $P < 0.01$). (F) Immunoblotting of A549-TIGAR-NLS or A549-parental xenografts tumors after 30 days of treatment with vehicle or doxorubicin.
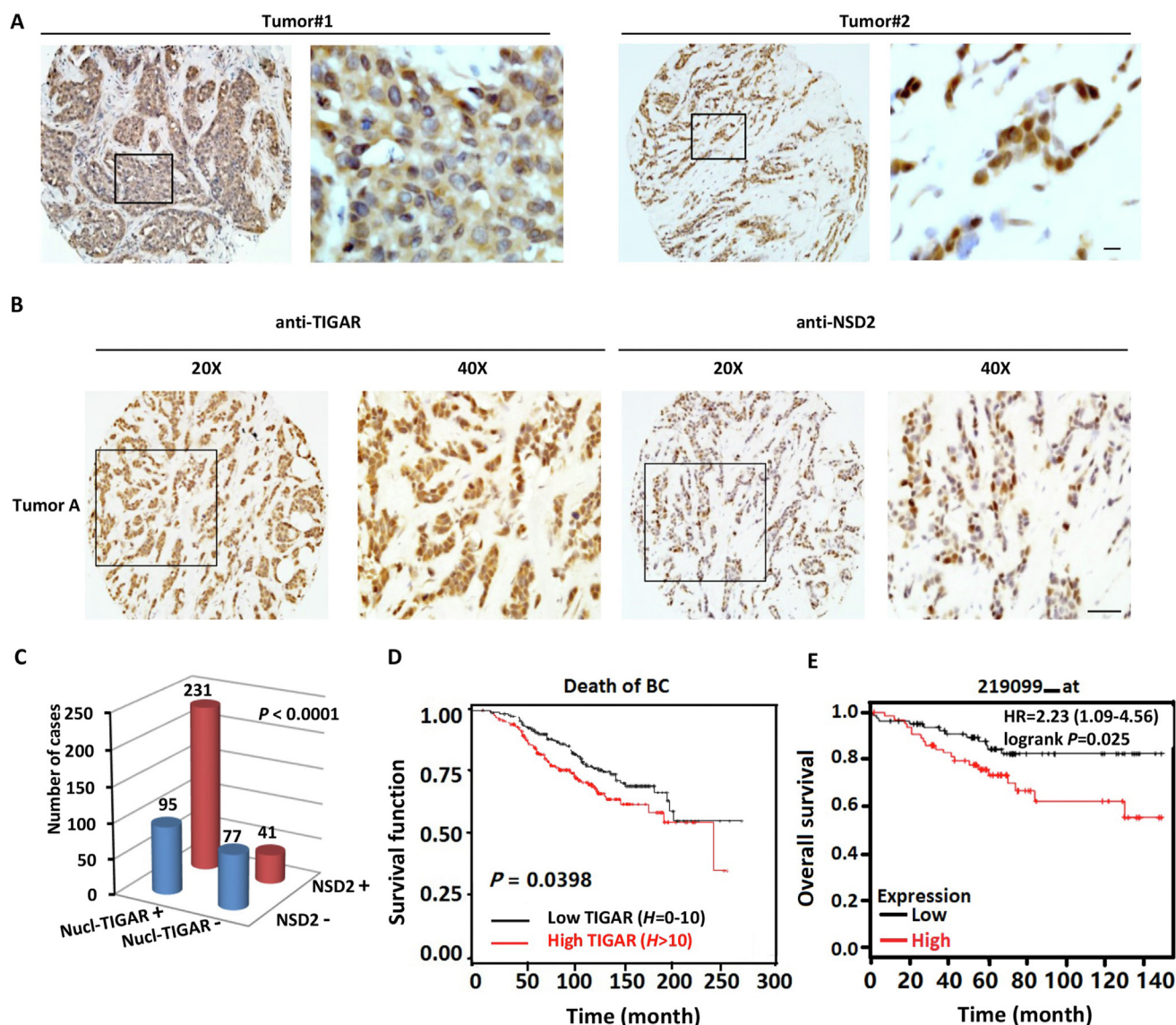
Figure 6 Nuclear TIGAR strongly correlates with NSD2 expression and patient poor survival. (A) and (B) Anti-TIGAR IHC analysis was performed on breast cancer TMAs. Representative images of cytoplasmic and nuclear staining in different tumors are shown (Top). Scale bar: 50 μm. (C) Correlations between nuclear TIGAR expression and NSD2 expression in the tumors was analyzed using Pearson's χ^2 test. (D) Kaplan−Meier analysis of overall survival from death due to breast cancer and recurrence-free survival of patients who received tamoxifen monotherapy ($n = 444$) and were stratified by tumor nuclear TIGAR protein levels determined by IHC. (E) Kaplan−Meier survival curve analysis of breast cancer patients, stratified by TIGAR expression (data were obtained from http://kmplot.com/analysis/).

different intensities, in addition to their cytoplasmic staining (Fig. 6A, tumor #2, and Supporting Information Fig. S6A). Consistent with the *in vitro* data that TIGAR controls the expression of NSD2, we found that nuclear TIGAR expression was strongly associated with the expression of NSD2 in the tumors (Fig. 6B and C, $P < 0.0001$). Importantly, when nuclear TIGAR staining was scored for the tumors, high levels of nuclear TIGAR were found to associate with a significantly shorter overall survival of the patients who received tamoxifen monotherapy (Fig. 6D, $P = 0.0398$). Moreover, analysis of published tumor datasets also showed a significant correlation between high tumor *TIGAR* mRNA level and poor overall survival of breast cancer patients subsequently treated with tamoxifen and of lung cancer patients (Fig. 6E and Fig. S6B). Together, these results suggest

that nuclear TIGAR strongly correlated with NSD2 expression and poor survival in cancer patients.

4. Discussion

Increasing evidence shows that both epigenetic and metabolic reprogramming are involved in redox homeostasis[1,28,31,41,42]. However, the underlying mechanism by which they coordinate in promoting cancer cell survival and drug resistance remains poorly understood. Here, we reveal that nuclear TIGAR coactivated the redox master regulator NRF2 to promote cancer therapeutic resistance *via* mediating the expression and function of NSD2, an oncogenic histone methylase. TIGAR has been characterized as a F2,6BPase with functions in dampening glycolysis and enhancing

the PPP to protect cells from damage induced by oxidative stress. In this study, we unexpectedly found that TIGAR can act as a transcriptional regulator. Nuclear TIGAR is readily detected by different approaches and observed in different types of cancer cells and tumors (*e.g.*, radiation-resistant and tamoxifen-resistant breast cancer cells and tumors and chemo-resistant lung cancer cells), with a marked increase in cells resistant to therapy. Importantly, ectopic expression of nuclear TIGAR conferred cancer chemotherapy resistance both *in vivo* and *in vitro*. Mechanistically, we demonstrated that TIGAR physically interacts with NRF2 and promotes NRF2 nuclear localization. Our further mechanistic study revealed that TIGAR can act as a novel coactivator of NRF2 to elevate the expression of both its new (*i.e.*, NSD2) and established (*e.g.*, NQO1/2, PRDX1 and GSTM4) targets. These data collectively suggest that nuclear TIGAR is a critical mediator in the NRF2 signaling.

Constitutive NRF2 activation plays a central role in anti-cancer therapy resistance. An increasing number of regulators of NRF2 pathway are being identified[28−30,43]. TIGAR is rather unusual in that it is a glucose metabolic enzyme and shares a key function with NRF2, namely stimulating the PPP for cellular redox control[12,25,28]. However, except a brief report on the distinct effect of a porphyrin-loaded nanoparticles on the mRNA levels of NRF2 and *TIGAR*[44], there has not been any studies on the physical and functional associations between NRF2 and TIGAR. Our study revealed that TIGAR is not only a coactivator of NRF2, it is also a downstream target of NRF2, thus clearly underscoring the crucial role of TIGAR in NRF2 signaling. Our previous study demonstrated that NSD2 can reprogram glucose metabolism for therapeutic resistance *via* coordinately up-regulating the expression of key metabolic enzymes for PPP and TIGAR[1]. Together with this study, our data suggest there is a positive, autoregulatory loop between TIGAR and NSD2 in mediating cancer therapeutic resistance. Such tight connections among the three proteins underscore the pivotal role of TIGAR−NRF2−NSD2 axis in effective and sustained reprogramming of cancer cell metabolism and epigenetics for therapeutic resistance. Mechanistically, we found that TIGAR is required for binding of NRF2 to its chromatin site and for active transcription marks (*i.e.*, H3K4me3) and transcription-competent Pol-II at the NSD2 promoter, providing important insights into the function of both NRF2 and TIGAR. Using recombinant proteins, we identified the C-terminal Neh1−Neh3 region of 170 amino acids being the specific region of NRF2 to interact with TIGAR. Interestingly, this C-terminal region also mediates interaction of NRF2 with its heterodimerization partners such as the small MAF proteins[45]. Therefore, it is possible that this C-terminal region of NRF2 can interact simultaneously with the small MAFs and TIGAR. Consistent with this proposition, we observed that TIGAR is important for the recruitment of NRF2 partner MAFF and MAFG to the NRF2 target. Moreover, we found that the F2,6bPase activity of TIGAR appears to be dispensable for it to act as a NRF2 coactivator, suggesting that its dual functions as a metabolic enzyme and transcriptional regulator can be uncoupled, which can be relevant for future therapeutics development targeting TIGAR.

The regulation of nuclear translocation of TIGAR is unclear at this point. TIGAR does not contain a readily recognizable nuclear localization signal sequence. Intriguingly, in Tam sensitive cells, TIGAR does not appear critical for NSD2 expression, pointing to the TIGAR−NSD2 axis being a unique mechanism that can develop during cancer therapeutic resistance. Although elevated NSD2 enhances its nuclear level, it is likely that nuclear translocation of TIGAR is subject to multiple ways of modulation. Similar to TIGAR, a nuclear form of PKM2 was described to function as a co-activator for HIF1α, β-catenin and others, and is subject to regulation by growth factors[46−51]. However, one distinction between them is that nuclear TIGAR promotes metabolic flux through the PPP for countering increased ROS and enhancing tumor resistance to therapies while nuclear PKM2 facilitates aerobic glycolysis for cell proliferation and tumor growth. Nevertheless, better understanding of the evolution of TIGAR−NRF2−NSD2 axis will provide valuable insights for developing strategies to disrupt the metabolic-epigenetic loops for more effective cancer therapy.

5. Conclusions

We report here that elevated TIGAR, an antioxidant, glucose metabolic regulator and a target of oncogenic histone methyltransferase NSD2, is mainly localized in the nucleus of therapeutic resistant tumor cells where it facilitates the recruitment of NRF2 to up-regulate antioxidant target genes including *NSD2*. In addition, nuclear accumulation of TIGAR is positively associated with NSD2 in clinical tumors and strongly correlated with poor survival. These findings define a nuclear TIGAR-mediated epigenetic autoregulatory loop in redox rebalance for tumor therapeutic resistance.

Author contributions

Hong Wang, Zhijian Duan, Qianqian Wang, Guodi Cai, Jie Huang, Jianwei Zheng and Junjian Wang designed and performed experiments and analyzed data. Alexander D. Borowsky performed the histopathological analyses. Jian Jian Li provided critical reagents and performed experiments. Zoann Nugent, Leigh Murphy and Peiqing Liu provided critical reagents and performed data analysis. Junjian Wang, Hsing-Jien Kung, and Hong-Wu Chen conceived and designed the study, and wrote the paper. Junjian Wang and Hong-Wu Chen jointly directed the project.

Conflicts of interest

The authors declare no conflicts of interest.

Appendix A.   Supporting information

Supporting data to this article can be found online at https://doi.org/10.1016/j.apsb.2021.10.015.

References

1. Wang J, Duan Z, Nugent Z, Zou JX, Borowsky AD, Zhang Y, et al. Reprogramming metabolism by histone methyltransferase NSD2 drives endocrine resistance *via* coordinated activation of pentose phosphate pathway enzymes. *Cancer Lett* 2016;**378**:69—79.
2. Achinger-Kawecka J, Valdes-Mora F, Luu PL, Giles KA, Caldon CE, Qu W, et al. Epigenetic reprogramming at estrogen-receptor binding sites alters 3D chromatin landscape in endocrine-resistant breast cancer. *Nat Commun* 2020;**11**:320.
3. Reina-Campos M, Linares JF, Duran A, Cordes T, L'Hermitte A, Badur MG, et al. Increased serine and one-carbon pathway metabolism by PKCλι deficiency promotes neuroendocrine prostate cancer. *Cancer Cell* 2019;**35**:385—400.e9.
4. Guièze R, Liu VM, Rosebrock D, Jourdain AA, Hernández-Sánchez M, Martinez Zurita A, et al. Mitochondrial reprogramming underlies resistance to BCL-2 inhibition in lymphoid malignancies. *Cancer Cell* 2019;**36**:369—84.e13.
5. Lauring J, Abukhdeir AM, Konishi H, Garay JP, Gustin JP, Wang Q, et al. The multiple myeloma associated *MMSET* gene contributes to cellular adhesion, clonogenic growth, and tumorigenicity. *Blood* 2008;**111**:856—64.
6. Hudlebusch HR, Santoni-Rugiu E, Simon R, Ralfkiaer E, Rossing HH, Johansen JV, et al. The histone methyltransferase and putative oncoprotein MMSET is overexpressed in a large variety of human tumors. *Clin Cancer Res* 2011;**17**:2919—33.
7. Yang P, Guo L, Duan ZJ, Tepper CG, Xue L, Chen X, et al. Histone methyltransferase NSD2/MMSET mediates constitutive NF-kappaB signaling for cancer cell proliferation, survival, and tumor growth *via* a feed-forward loop. *Mol Cell Biol* 2012;**32**:3121—31.
8. Cai D, Wang J, Gao B, Li J, Wu F, Zou JX, et al. RORγ is a targetable master regulator of cholesterol biosynthesis in a cancer subtype. *Nat Commun* 2019;**10**:4621.
9. Fang P, De Souza C, Minn K, Chien J. Genome-scale CRISPR knockout screen identifies TIGAR as a modifier of PARP inhibitor sensitivity. *Commun Biol* 2019;**2**:335.
10. Feng Q, Zhang Z, Shea MJ, Creighton CJ, Coarfa C, Hilsenbeck SG, et al. An epigenomic approach to therapy for tamoxifen-resistant breast cancer. *Cell Res* 2014;**24**:809—19.
11. Wang Q, Zheng J, Zou JX, Xu J, Han F, Xiang S, et al. *S*-Adenosylhomocysteine (AdoHcy)-dependent methyltransferase inhibitor DZNep overcomes breast cancer tamoxifen resistance *via* induction of NSD2 degradation and suppression of NSD2-driven redox homeostasis. *Chem Biol Interact* 2020;**317**:108965.
12. Bensaad K, Tsuruta A, Selak MA, Vidal MN, Nakano K, Bartrons R, et al. TIGAR, a p53-inducible regulator of glycolysis and apoptosis. *Cell* 2006;**126**:107—20.
13. Zhang DM, Zhang T, Wang MM, Wang XX, Qin YY, Wu J, et al. TIGAR alleviates ischemia/reperfusion-induced autophagy and ischemic brain injury. *Free Radic Biol Med* 2019;**137**:13—23.
14. Geng J, Wei M, Yuan X, Liu Z, Wang X, Zhang D, et al. TIGAR regulates mitochondrial functions through SIRT1—PGC1α pathway and translocation of TIGAR into mitochondria in skeletal muscle. *Faseb J* 2019;**33**:6082—98.
15. Wang H, Cheng Q, Li X, Hu F, Han L, Zhang H, et al. Loss of TIGAR induces oxidative stress and meiotic defects in oocytes from obese mice. *Mol Cell Proteomics* 2018;**17**:1354—64.
16. Cheung EC, Athineos D, Lee P, Ridgway RA, Lambie W, Nixon C, et al. TIGAR is required for efficient intestinal regeneration and tumorigenesis. *Dev Cell* 2013;**25**:463—77.
17. Shen M, Zhao X, Zhao L, Shi L, An S, Huang G, et al. Met is involved in TIGAR-regulated metastasis of non-small-cell lung cancer. *Mol Cancer* 2018;**17**:88.
18. Geng J, Yuan X, Wei M, Wu J, Qin ZH. The diverse role of TIGAR in cellular homeostasis and cancer. *Free Radic Res* 2018;**52**:1240—9.
19. Hong M, Xia Y, Zhu Y, Zhao HH, Zhu H, Xie Y, et al. TP53-induced glycolysis and apoptosis regulator protects from spontaneous apoptosis and predicts poor prognosis in chronic lymphocytic leukemia. *Leuk Res* 2016;**50**:72—7.
20. Wei M, Peng J, Wu P, Chen P, Yang H, Cui Y, et al. Prognostic value of TIGAR and LC3B protein expression in nasopharyngeal carcinoma. *Cancer Manag Res* 2018;**10**:5605—16.
21. Wang X, Li R, Chen R, Huang G, Zhou X, Liu J. Prognostic values of TIGAR expression and ^{18}F-FDG PET/CT in clear cell renal cell carcinoma. *J Cancer* 2020;**11**:1—8.
22. Shah MY, Martinez-Garcia E, Phillip JM, Chambliss AB, Popovic R, Ezponda T, et al. MMSET/WHSC1 enhances DNA damage repair leading to an increase in resistance to chemotherapeutic agents. *Oncogene* 2016;**35**:5905—15.
23. Zhang Y, Chen F, Tai G, Wang J, Shang J, Zhang B, et al. TIGAR knockdown radiosensitizes TrxR1-overexpressing glioma *in vitro* and *in vivo via* inhibiting Trx1 nuclear transport. *Sci Rep* 2017;**7**:42928.
24. Chu J, Niu X, Chang J, Shao M, Peng L, Xi Y, et al. Metabolic remodeling by TIGAR overexpression is a therapeutic target in esophageal squamous-cell carcinoma. *Theranostics* 2020;**10**:3488—502.
25. Cheung EC, DeNicola GM, Nixon C, Blyth K, Labuschagne CF, Tuveson DA, et al. Dynamic ROS control by TIGAR regulates the initiation and progression of pancreatic cancer. *Cancer Cell* 2020;**37**:168—82.e4.
26. Cheung EC, Ludwig RL, Vousden KH. Mitochondrial localization of TIGAR under hypoxia stimulates HK2 and lowers ROS and cell death. *Proc Natl Acad Sci U S A* 2012;**109**:20491—6.
27. Yu HP, Xie JM, Li B, Sun YH, Gao QG, Ding ZH, et al. TIGAR regulates DNA damage and repair through pentosephosphate pathway and Cdk5—ATM pathway. *Sci Rep* 2015;**5**:9853.
28. Rojo de la Vega M, Chapman E, Zhang DD. NRF2 and the hallmarks of cancer. *Cancer Cell* 2018;**34**:21—43.
29. Cuadrado A, Rojo AI, Wells G, Hayes JD, Cousin SP, Rumsey WL, et al. Therapeutic targeting of the NRF2 and KEAP1 partnership in chronic diseases. *Nat Rev Drug Discov* 2019;**18**:295—317.
30. Ge W, Zhao K, Wang X, Li H, Yu M, He M, et al. iASPP is an antioxidative factor and drives cancer growth and drug resistance by competing with Nrf2 for Keap1 binding. *Cancer Cell* 2017;**32**:561.
31. Mukhopadhyay S, Goswami D, Adiseshaiah PP, Burgan W, Yi M, Guerin TM, et al. Undermining glutaminolysis bolsters chemotherapy while NRF2 promotes chemoresistance in KRAS-driven pancreatic cancers. *Cancer Res* 2020;**80**:1630—43.
32. Guo L, Xiao Y, Fan M, Li JJ, Wang Y. Profiling global kinome signatures of the radioresistant MCF-7/C6 breast cancer cells using MRM-based targeted proteomics. *J Proteome Res* 2015;**14**:193—201.
33. Yi W, Clark PM, Mason DE, Keenan MC, Hill C, Goddard WA, et al. Phosphofructokinase 1 glycosylation regulates cell growth and metabolism. *Science* 2012;**337**:975—80.
34. Kim JH, Yu S, Chen JD, Kong AN. The nuclear cofactor RAC3/AIB1/SRC-3 enhances Nrf2 signaling by interacting with transactivation domains. *Oncogene* 2013;**32**:514—27.
35. Dalal S, Rosser MFN, Cyr DM, Hanson PI. Distinct roles for the AAA ATPases NSF and p97 in the secretory pathway. *Mol Biol Cell* 2004;**15**:637—48.
36. Snell L, Watson PH. Breast tissue banking: collection, handling, storage, and release of tissue for breast cancer research. *Methods Mol Med* 2006;**120**:3—24.
37. Shrivastav A, Bruce M, Jaksic D, Bader T, Seekallu S, Penner C, et al. The mechanistic target for rapamycin pathway is related to the

phosphorylation score for estrogen receptor-alpha in human breast tumors *in vivo*. *Breast Cancer Res* 2014;**16**:R49.

38. Gyorffy B, Lanczky A, Eklund AC, Denkert C, Budczies J, Li Q, et al. An online survival analysis tool to rapidly assess the effect of 22,277 genes on breast cancer prognosis using microarray data of 1,809 patients. *Breast Cancer Res Treat* 2010;**123**:725−31.

39. Hayes JD, Dinkova-Kostova AT. The Nrf2 regulatory network provides an interface between redox and intermediary metabolism. *Trends Biochem Sci* 2014;**39**:199−218.

40. Won KY, Lim SJ, Kim GY, Kim YW, Han SA, Song JY, et al. Regulatory role of p53 in cancer metabolism *via* SCO2 and TIGAR in human breast cancer. *Hum Pathol* 2012;**43**:221−8.

41. Bazopoulou D, Knoefler D, Zheng Y, Ulrich K, Oleson BJ, Xie L, et al. Developmental ROS individualizes organismal stress resistance and lifespan. *Nature* 2019;**576**:301−5.

42. Pal A, Chiu HY, Taneja R. Genetics, epigenetics and redox homeostasis in rhabdomyosarcoma: emerging targets and therapeutics. *Redox Biol* 2019;**25**:101124.

43. Liu Y, Tao S, Liao L, Li Y, Li H, Li Z, et al. TRIM25 promotes the cell survival and growth of hepatocellular carcinoma through targeting Keap1−Nrf2 pathway. *Nat Commun* 2020;**11**:348.

44. Canaparo R, Varchi G, Ballestri M, Foglietta F, Sotgiu G, Guerrini A, et al. Polymeric nanoparticles enhance the sonodynamic activity of meso-tetrakis (4-sulfonatophenyl) porphyrin in an *in vitro* neuroblastoma model. *Int J Nanomed* 2013;**8**:4247−63.

45. Song MY, Lee DY, Chun KS, Kim EH. The role of NRF2/KEAP1 signaling pathway in cancer metabolism. *Int J Mol Sci* 2021;**22**:4376.

46. Lv L, Xu YP, Zhao D, Li FL, Wang W, Sasaki N, et al. Mitogenic and oncogenic stimulation of K433 acetylation promotes PKM2 protein kinase activity and nuclear localization. *Mol Cell* 2013;**52**:340−52.

47. Yang W, Xia Y, Ji H, Zheng Y, Liang J, Huang W, et al. Nuclear PKM2 regulates beta-catenin transactivation upon EGFR activation. *Nature* 2011;**480**:118−22.

48. Luo W, Hu H, Chang R, Zhong J, Knabel M, O'Meally R, et al. Pyruvate kinase M2 is a PHD3-stimulated coactivator for hypoxia-inducible factor 1. *Cell* 2011;**145**:732−44.

49. Chen TJ, Wang HJ, Liu JS, Cheng HH, Hsu SC, Wu MC, et al. Mutations in the PKM2 exon-10 region are associated with reduced allostery and increased nuclear translocation. *Commun Biol* 2019;**2**:105.

50. Bhardwaj A, Das S. SIRT6 deacetylates PKM2 to suppress its nuclear localization and oncogenic functions. *Proc Natl Acad Sci U S A* 2016;**113**:E538−47.

51. Gowda P, Patrick S, Singh A, Sheikh T, Sen E. Mutant isocitrate dehydrogenase 1 disrupts PKM2−β-Catenin−BRG1 transcriptional network-driven CD47 expression. *Mol Cell Biol* 2018;**38**:e00001−18.